JOURNAL OF APPLIED ELECTROCHEMISTRY 9 (1979) 125–139

Impedance parameters and the state-of-charge. I. Nickel-cadmium battery

S. SATHYANARAYANA, S. VENUGOPALAN*, M. L. GOPIKANTH

Department of Inorganic and Physical Chemistry, Indian Institute of Science, Bangalore, India

Received 5 May 1978

The problem of nondestructive determination of the state-of-charge of nickel–cadmium batteries has been examined experimentally as well as theoretically from the viewpoint of internal impedance. It is shown that the modulus of the impedance is mainly controlled by diffusion at all states of charge. Even so, a prediction of the state of charge is possible if the equivalent series/parallel capacitance or the alternating current phase shift is measured at a sufficiently low a.c. test frequency (5–30 Hz) which also avoids inductive effects. These results are explained on the basis of a uniform transmission-line analog equivalent circuit for the battery electrodes.

1. Introduction

The state-of-charge of a battery refers to the ratio of residual capacity at a given instant to the maximum capacity available from the battery. A knowledge of the state-of-charge not only helps in predicting the residual capacity, but also helps in increasing the life expectancy of the battery by proper utilization. The latter result is due to the fact that the number of charge–discharge cycles which a rechargeable battery can undergo is determined by the difference in the states-of-charge at the end of charge and at the end of discharge in each cycle.

Many attempts have been made in the literature to determine the state-of-charge of a battery by measurement of properties such as dissolved-ion concentration [1], open-circuit voltage, closed-circuit voltage, internal resistance [2–6]†, open-circuit voltage recovery transient [8], alternating current phase shift [1, 9], alternating current impedance and its components [4, 10, 11], current-sharing [1] and coulometric method [12].

An analysis of the above literature indicates that the methods proposed for the nondestructive determination of the state-of-charge, especially with respect to the nickel–cadmium battery, have been either unsuccessful or have often given conflicting results. Moreover, the results obtained have not always been interpreted from a fundamental angle in a way that the effects of ageing or charge–discharge cycling etc., could be predicted and allowed for.

In the present work, the problem of nondestructive determination of the state-of-charge of the nickel–cadmium battery has been re-examined experimentally and the results interpreted theoretically using an idealized model for the porous electrodes of the battery.

Preliminary studies indicated that the open-circuit voltage and the open-circuit voltage recovery transient of the battery are not sufficiently sensitive to variations in the state-of-charge. Hence, a detailed study was restricted to the measurement and interpretation of the parameters of the internal impedance at various test frequencies and states of charge.

2. Experimental

2.1. *Cells*

The nickel–cadmium cells were of sintered plate pressure-vented design (4 Ah nominal capacity)

* On leave from Tamil Nadu Alkaline Batteries Ltd, Madras, India.

† Methods of measurement of internal resistance of batteries by a.c., d.c. and pulse methods have been recently reviewed [7].

manufactured by Tamil Nadu Alakaline Batteries Ltd, Madras (India). The cells were subjected to three 'conditioning' cycles of charge–discharge and then matched so that the capacities were within 5% of the mean. Three such matched cells were used for the tests.

2.2. *Procedure*

The cells were subjected to one deep charge–discharge cycle before the tests began. This has the effect of activating the surfaces of the electrodes and making their performance reproducible.

It was found during preliminary experiments that when cells are charged or discharged, as the case may be, several hours are required after the termination of charge or discharge so that the open-circuit voltage became constant with time, i.e., equilibrium was re-established. Thus, cells at different states-of-charge were obtained as follows.

Since the absolute capacity (C) was known by earlier charge–discharge studies, a predetermined amount of charge was withdrawn by discharge at constant current (or introduced by charging at constant current) at the ten-hour rate ($C/10$) followed by a ten-hour rest period was given before the measurements began.

2.3. *Set-up*

Impedance parameters were measured using the a.c. bridge method. Since a charged nickel–cadmium cell is a direct current power source, modifications are necessary in the design of the a.c. bridge. Earlier attempts in this direction have been recently reviewed [7, 13].

The circuit adopted is shown in Fig. 1. It is essentially of the Wien bridge type. The cells were connected to the test circuit through firm, large-area contacts. The high-resistance ratio arms ensured a negligible discharge of the battery during the measurements. Appropriate tappings on this arm were provided to get different ratios so that the cell impedance was brought within the range of the components in the balancing arm. The balancing arm with a parallel RC connection ensured an easier bridge balance with the available components.

The lock-in amplifier displayed both the in-phase and quadrature components. It was employed in the differential mode so that the

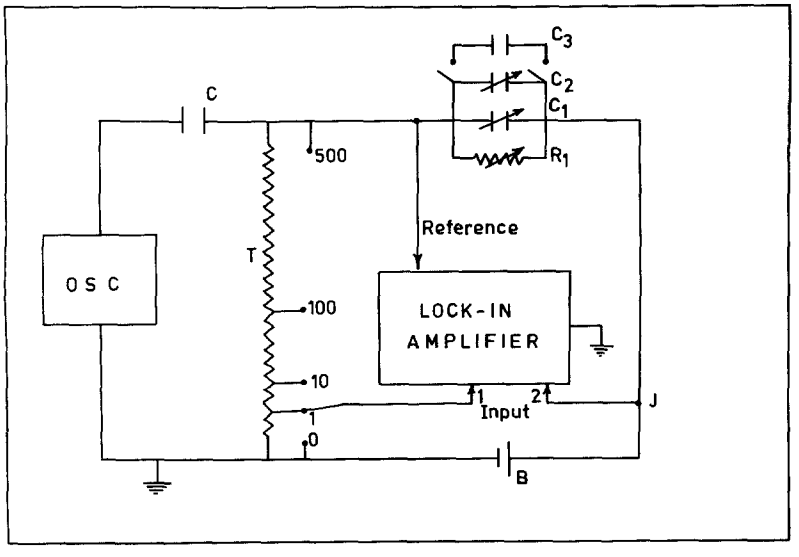

Fig. 1. Circuit diagram of the alternating current bridge circuit to measure impedance of batteries or cells. OSC, low frequency signal generator; C, blocking capacitor (10^3 μF, 100 V d.c.); B, test battery or cell; T, ratio arm of total resistance 50 kΩ with tappings at 100 Ω, 1 kΩ and 50 kΩ; R_1, decade resistance box (GR, 0·1–11 111·11 Ω in steps of 0·1 Ω); C_1, decade capacitance box (GR, 100 pF–1·111 μF in steps of 0·0001 μF); C_2, decade capacitance box (Radart, 50 pF–11·111 μF in steps of 0·0001 μF); C_3, standard polyester capacitor (10 μF). Vector lock-in amplifier: PAR, Model 129A.

balance point could be accurately obtained. The maximum sensitivity of the lock-in amplifier was about 2 μV which enabled the excitation signal across the test cell to be kept as small as 1 mV.* The overall accuracy of the bridge measurement was found to be better than 0·5% using standard R–C components. From the measured values of the equivalent parallel components R_p and C_p, other parameters of the cell impedance were computed using the following formulae.

Equivalent series resistance

$$R_s = [R_p/(1 + \omega^2 R_p^2 C_p^2)] \quad (1)$$

Equivalent series capacitance

$$C_s = C_p [1 + 1/(\omega^2 R_p^2 C_p^2)] \quad (2)$$

Modulus of impedance

$$|Z| = [R_s^2 + 1/(\omega^2 C_s^2)]^{1/2} \quad (3)$$

Alternating current phase shift

$$\phi = \tan^{-1}(\omega R_p C_p) \quad (4)$$

where $\omega = 2\pi f$, f being the frequency (Hz).

3. Results

At an alternating current frequency of 40 Hz or more, the inductive reactance of the cells became prominent, as indicated by the tendency of C_p to become negative at the balancing point. This is apparently due to the fact that the electrode structures are made of sintered nickel which is a ferromagnetic substance and the active material (nickel hydroxide) of the positive electrode is itself a paramagnetic compound. Since the inductive and capacitive components of the cell could not be separated, the impedance measurements were restricted to an a.c. frequency less than 30 Hz. The lowest frequency that could be used was governed by the available range of C_p in the balancing arm. As the a.c. frequency is decreased the required value of C_p increases sharply below about 10 Hz, thus the a.c. frequency range adopted was 5–30 Hz.

The results thus obtained with regard to equivalent series resistance (R_s), equivalent parallel resistance (R_p) and modulus of impedance ($|Z|$) as a function of a.c. frequency are shown in Fig. 2. It is seen that except for a slight decrease of these parameters with an increase in frequency there are no outstanding features on the curves.

The dependence of R_p, R_s and $|Z|$ at different a.c. frequencies on the state-of-charge of the nickel–cadmium cells is shown in Fig. 3. Apart from a fairly sharp change between S (the state-of-charge) = 0·8 and S = 0·6, the values are more or less constant in the remaining region. There is no particular trend of the curves that seems useful for the prediction of state-of-charge.

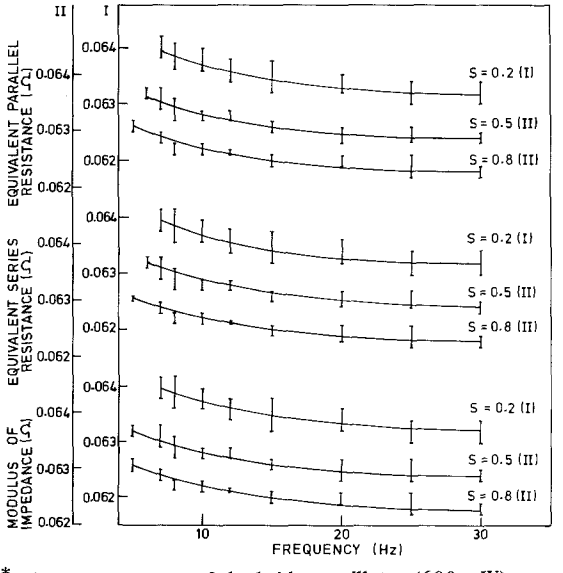

Fig. 2. Dependence of equivalent parallel resistance (R_p), equivalent series resistance (R_s) and modulus of impedance $|Z|$ on frequency at different states-of-charge.

* The power output of the bridge oscillator (600 mW) was adequate to maintain distortionless signal amplitudes up to 10 mV (P–P) across the cell without the aid of a potentiostat.

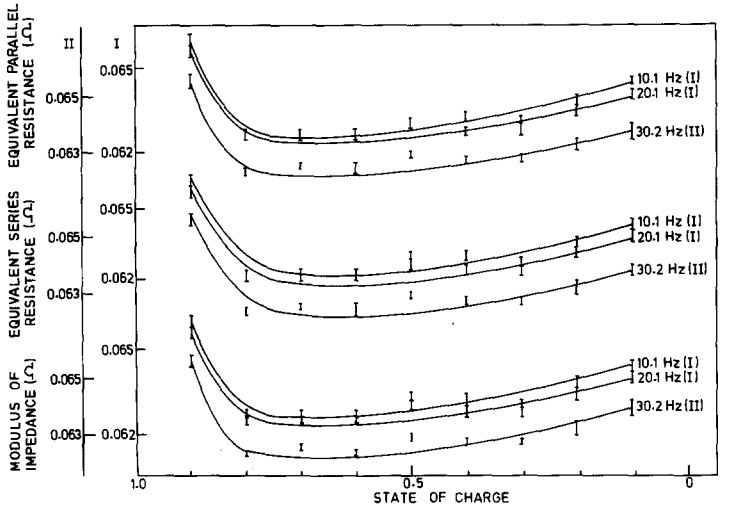

Fig. 3. Dependence of equivalent parallel resistance (R_p), equivalent series resistance (R_s) and modulus of impedance ($|Z|$) on state-of-charge at different frequencies.

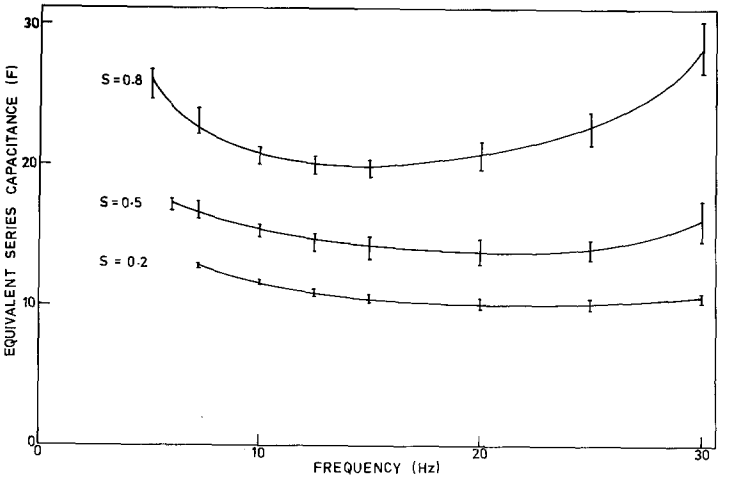

Fig. 4. Dependence of equivalent series capacitance (C_s) on frequency at different states-of-charge.

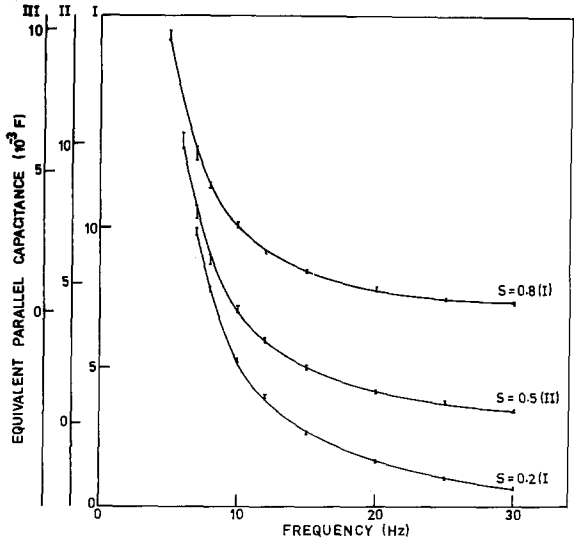

Fig. 5. Dependence of equivalent parallel capacitance (C_p) on frequency of nickel at different states-of-charge.

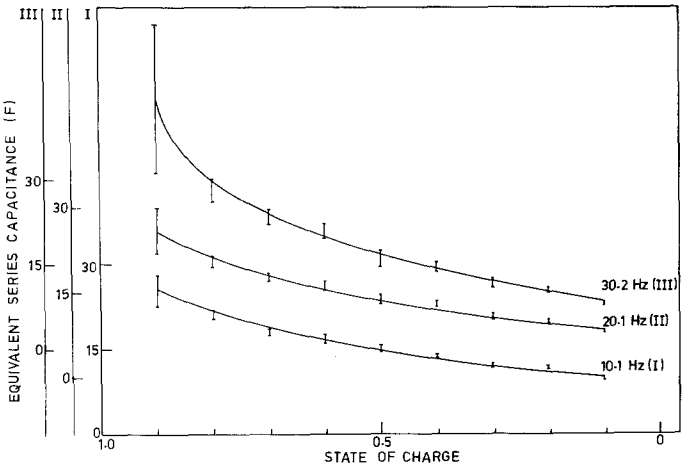

Fig. 6. Dependence of equivalent series capacitance (C_s) on state-of-charge at different frequencies.

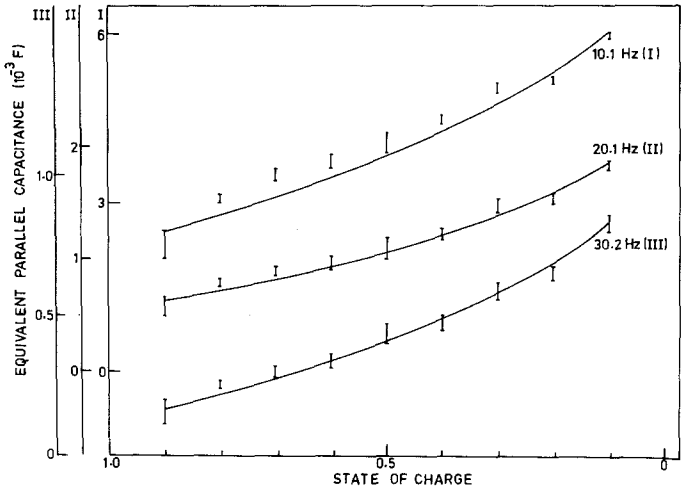

Fig. 7. Dependence of equivalent parallel capacitance (C_p) on state-of-charge at different frequencies.

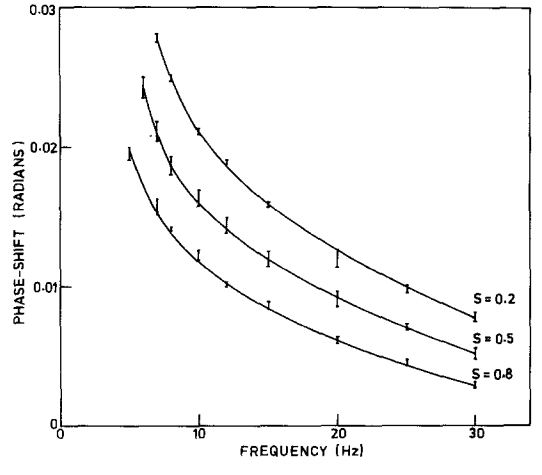

Fig. 8. Dependence of phase shift (ϕ) on frequency at different states-of-charge.

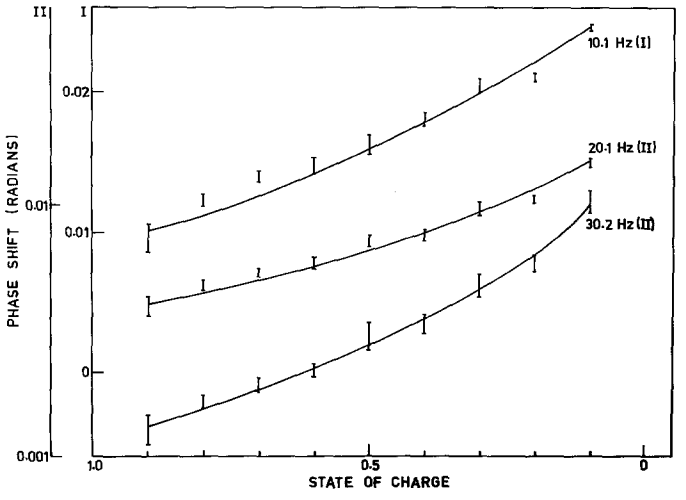

Fig. 9. Dependence of phase shift (ϕ) on state-of-charge at different frequencies.

The equivalent series capacitance (C_s) and equivalent parallel capacitance (C_p) vary with a.c. frequency in different ways as shown in Figs. 4 and 5, respectively. While C_p versus frequency shows a steady fall, C_s versus frequency exhibits a flat minimum. However, the dependence of C_p and C_s on the states-of-charge of the cell shows a steady change (Figs. 6 and 7) in both the cases, C_s decreasing and C_p increasing with a decrease in the state-of-charge.

The phase angle between the alternating voltage across the cell and alternating current through the cell is found to decrease with a.c. frequency (Fig. 8) at a given state-of-charge. The phase angle increases almost linearly with a decrease in the state-of-charge (Fig. 9).

4. Discussion

As a circuit element, a galvanic cell (or a battery) may always be represented [14] as an ideal voltage source (i.e., without any internal impedance) in series with a combination of a reactance (usually capacitive) and a resistance in either a parallel mode ($R_p - C_p$) or a series mode ($R_s - C_s$) as shown in Fig. 10.

It then follows from circuit theory that the complex impedance of the battery is given by

$$Z = [R_s + (1/j\omega C_s)] = [R_p/(1 + j\omega C_p R_p)] \quad (5)$$

where $j = \sqrt{-1}$; $\omega = 2\pi f$, f being the frequency (Hz). The impedance of each electrode of a cell in

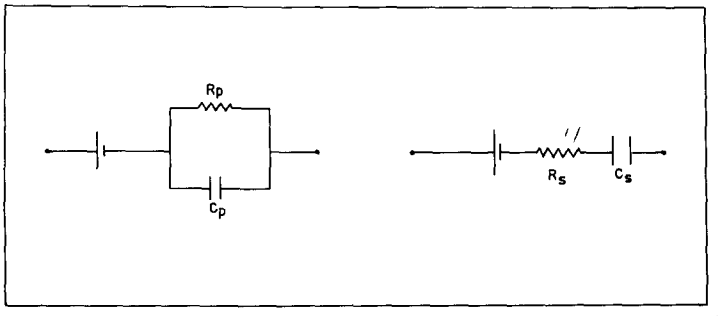

Rp = Equivalent parallel resistance
Rs = Equivalent series resistance
Cp = Equivalent parallel capacitance
Cs = Equivalent series capacitance

Fig. 10. Lumped equivalent circuit of a battery or cell as a circuit element.

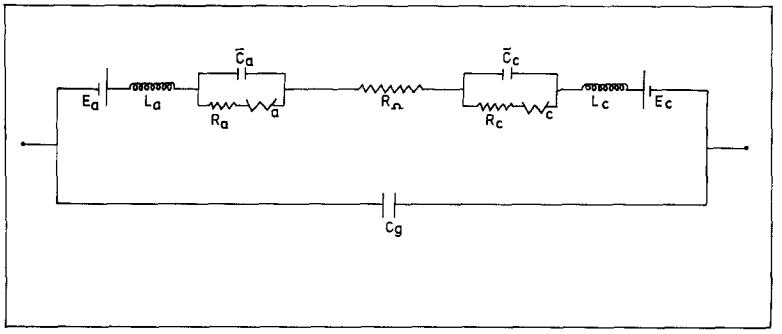

E_a, E_c = Single electrode potentials.
L_a, L_c = Lead inductances.
$\bar{C}_a$, $\bar{C}_c$ = Double layer capacitances.
R_a, R_c = Charge transfer resistances.
W_a, W_c = Diffusional (Warburg) impedance.
R_Ω = Resistance of solution and separator.
C_g = Interelectrode capacitance.

Fig. 11. Equivalent circuit of a battery or cell (subscripts a and c denote anode and cathode, respectively).

a battery will have a contribution from charge- and mass-transfer processes as well as from the double-layer capacitance and lead inductances. The electrolyte solution and separator will contribute resistance to the battery impedance. Finally, the battery electrodes will contribute a 'geometrical' capacitance due to their close parallel spacing. Taking into account the above facts and following the classical Randles' equivalent circuit for single electrodes [15], the equivalent circuit of a battery or a cell may be represented as shown in Fig. 11.

The following assumptions are made to simplify further analysis. Since the two electrodes (cathode and anode) of the battery behave similarly in principle, i.e., sustaining charge- and mass-transfer processes, the electrode impedance may be combined to give a single impedance consisting of new, effective values of double-layer capacitance ($\bar{C}$), charge-transfer resistance (R_t) and mass-transfer impedance (W) of the battery interconnected as for a single electrode. The actual expressions for these are unimportant for the present discussion.

By choosing a sufficiently low a.c. frequency for impedance measurements, it is possible to ensure, as shown in Section 3, that the inductive reactance is small compared to the capacitive reactance i.e., L_a, and L_c may be neglected in Fig. 11.

For practical battery systems, the geometrical capacitance is smaller than the measured capacitance by several orders. C_g may therefore be omitted from Fig. 11.

Thus the modified equivalent circuit of a cell may be represented as shown in Fig. 12.

The properties of the Randles-type impedance network in Fig. 12 have been thoroughly examined in the literature [15]. Thus, for the impedance of the circuit in Fig. 12

$$Z = [R_s - (j/\omega C_s)] \tag{6}$$

$$R_s = R_\Omega + \left[\frac{(R_t + \sigma/\sqrt{\omega})}{(1+\sqrt{\omega}\bar{C}\sigma)^2 + \omega^2\bar{C}^2\,(R_t + \sigma/\sqrt{\omega})^2}\right] \tag{7}$$

$$\frac{1}{\omega C_s} = \left[\frac{(\sigma/\sqrt{\omega})\,(1+\sqrt{\omega}\bar{C}\sigma) + \omega\bar{C}\,(R_t + \sigma/\sqrt{\omega})^2}{(1+\sqrt{\omega}\bar{C}\sigma)^2 + \omega^2\bar{C}^2\,(R_t + \sigma/\sqrt{\omega})^2}\right]. \tag{8}$$

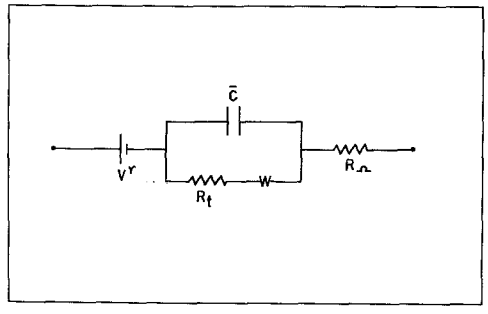

V^r = Ec – Ea = EMF of the battery
R_t = Charge transfer resistance
W = Diffusional (Warburg) impedance
$\bar{C}$ = Double layer capacitance
R_Ω = Resistance of solution and separator

Fig. 12. Equivalent circuit of a battery or cell (simplified).

where R_Ω is the solution resistance. The resistance and reactive parts of the Warburg impedance in Fig. 12 are taken into account in the above equation as

$$W = \left[\frac{\sigma}{\sqrt{\omega}} - j\frac{\sigma}{\sqrt{\omega}}\right] \quad (9)$$

where σ is the Warburg coefficient. The value of σ may be calculated for specific cases from diffusion theory. For example, when there is a linear diffusion of species O and R towards a plane electrode at the equilibrium potential of the reaction

$$O + ne \rightleftharpoons R \quad (10)$$

$$\sigma = \frac{RT}{n^2F^2A\sqrt{(2\omega)}} \times [(1/C_O^0\sqrt{D_O}) + (1/C_R^0\sqrt{D_R})] \quad (11)$$

where A is the active area of the electrode, C_O^0 and C_R^0 are the bulk concentration of the species O and R and D_O and D_R their diffusion coefficients. R is the gas constant, F Faraday constant and T absolute temperature. The expression for σ has to be modified when there is a direct current polarization of the electrode.

The charge-transfer resistance R_t is related to concentration term through the exchange current as

$$R_t = \left[\frac{RT}{nFI_0}\right] \quad (12)$$

where I_0 is the exchange current of the potential-determining reaction at the electrode.

It follows that, in a broad sense, R_t and σ are dependent on the state-of-charge of the battery through the concentration terms. Hence, from Equations 6–9, the impedance of the cell or battery as well as the related parameters R_s and C_s should also be dependent on the state of charge.

Due to the involved forms of Equations 7 and 8, special graphical methods have been developed to evaluate the various parameters. In particular, if $(1/\omega C_s)$ is plotted against R_s at various a.c. frequencies (Argand plots) it is found that the resulting curve is a straight line of unit slope and intercept at $[2\sigma^2\bar{C} - (R_\Omega + R_t)]$ (Equations 13–15) in the case of pure diffusion polarization ($\omega \to 0$) or a semicircle of diameter R_t (Equations 16–18) in the case of pure charge-transfer polarization ($\sigma \to 0$).

If $\omega \to 0$,

$$(1/\omega C_s) = (\sigma/\sqrt{\omega}) \quad (13)$$

$$R_s = R_\Omega + R_t + (\sigma/\sqrt{\omega}) - 2\sigma^2\bar{C} \quad (14)$$

$$(1/\omega C_s) = R_s + 2\sigma^2\bar{C} - R_\Omega - R_t . \quad (15)$$

If $\sigma \to 0$,

$$(1/\omega C_s) = \omega\bar{C}R_t^2/(1 + \omega^2\bar{C}^2R_t^2) \quad (16)$$

$$R_s = R_\Omega + R_t/(1 + \omega^2\bar{C}^2R_t^2) \quad (17)$$

$$(1/\omega^2C_s^2) + (R_s - R_\Omega - R_t/2)^2 = R_t^2/4 . \quad (18)$$

Assuming the validity of Randles' equivalent circuit for the electrodes, it is possible in principle to employ the limiting results such as Equations 13–18 to evaluate the parameters such as R_Ω, $\bar{C}$, R_t, or σ, establish the mechanism of the electrode reaction, and interpret any observed correlation between the state-of-charge of a cell, and the impedance parameters R_s, $(1/\omega C_s)$, $|Z|$ and ϕ.

Experimental data of $(1/\omega C_s)$ and R_s show that the Argand plots of $(1/\omega C_s)$ versus R_s for the nickel–cadmium cell system at different states-of-charge are fairly good straight lines (Fig. 13) with a slope of $1{\cdot}7 \pm 0{\cdot}01$.*

It is therefore reasonable to assume that diffusion is controlling the polarization impedance. The dominant role of diffusion is quite understandable because of the large rate constants at the cell electrodes. Notwithstanding the above explanations, it may be noticed that the slope of the $(1/\omega C_s)$ versus R_s straight lines is substantially larger than that predicted from Equation 15. It is, therefore, desirable to cross-check the model. For this purpose, plots of $(1/\omega C_s)$ versus $(1/\sqrt{\omega})$ and of R_s versus $(1/\sqrt{\omega})$ may be constructed (Equations 13 and 14). The plots of $(1/\omega C_s)$ versus $(1/\sqrt{\omega})$ (Figs. 14–16) at different states-of-charge reveal that the intercepts of the lines (Curves 2 in Figs. 14–16) on the reactance axis are large negative quantities, well beyond experimental error. Such a negative intercept has no physical meaning within the framework of Randles' model for the equivalent circuit. A similar plot of R_s versus $(1/\sqrt{\omega})$ (Fig. 17) is found to give a large positive intercept, which is essentially R_Ω in this case. However,

* The limiting slope predicted for a thick, flooded porous electrode is $\pi/8$ under certain conditions [17].

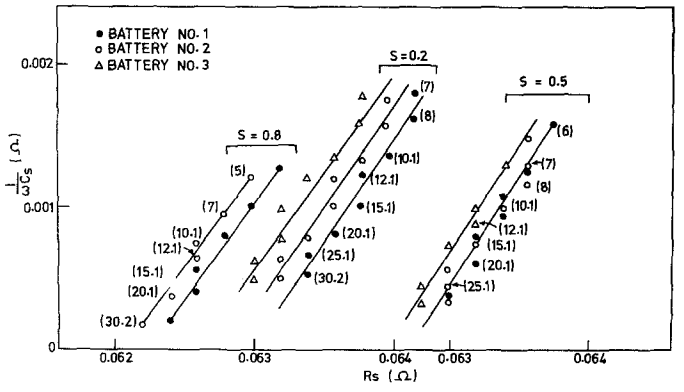

Fig. 13. Argand plots of nickel–cadmium cell at different states-of-charge. (The number on curves indicate frequency in Hz).

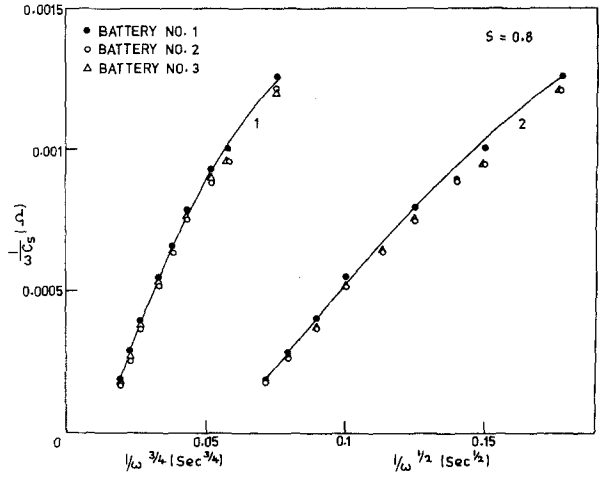

Fig. 14. Dependence of $(1/\omega C_s)$ on $(1/\omega^{1/2})$ (Curve 2) and on $(1/\omega^{3/4})$ (Curve 1) for nickel–cadmium cell at different states-of-charge (as indicated).

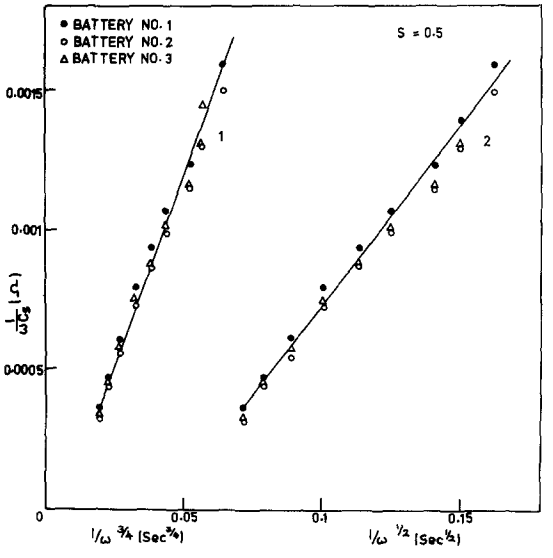

Fig. 15. Dependence of $(1/\omega C_s)$ on $(1/\omega^{1/2})$ (Curve 2) and on $(1/\omega^{3/4})$ (Curve 1) for nickel–cadmium cell at different states-of-charge (as indicated).

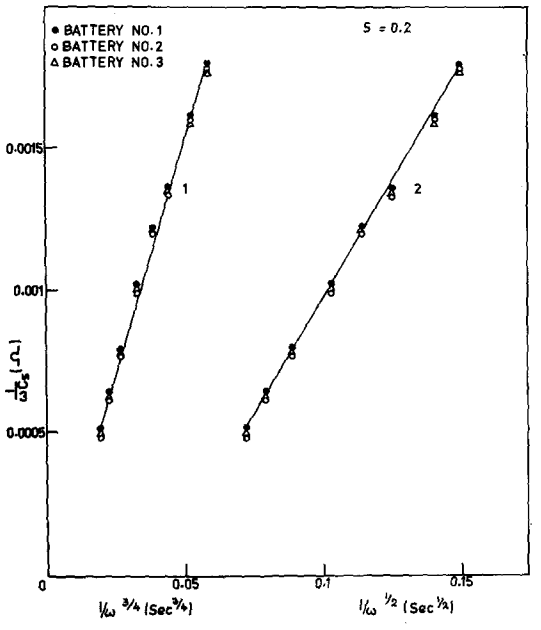

Fig. 16. Dependence of $(1/\omega C_S)$ on $(1/\omega^{1/2})$ (Curve 2) and on $(1/\omega^{3/4})$ (Curve 1) for nickel–cadmium cell at different states-of-charge (as indicated).

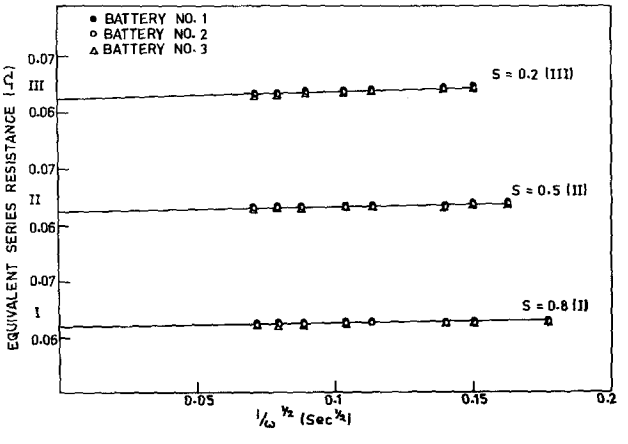

Fig. 17. Dependence of equivalent series resistance (R_S) on $(1/\omega^{1/2})$ at different states-of-charge.

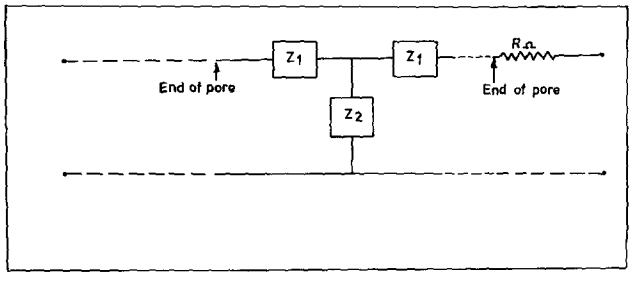

Fig. 18. Transmission-line model of a single pore in the porous electrodes of a cell or battery.

no further use of R_s versus $(1/\sqrt{\omega})$ plot is possible because R_Ω is much larger than the remaining terms in R_s and fluctuations in R_Ω (caused, for example, by a variable wetting of the separator and electrode pores by the solution) mask any trend of change of $(R_s - R_\Omega)$ with other variables.

It may therefore be concluded that whereas the impedance of the nickel–cadmium cell is mainly composed of diffusion impedance, refinements of the model are called for in order to explain all the impedance characteristics.

An obvious refinement to be considered is to incorporate the main features of the porous electrodes of which the cell or battery anode and cathode are made.

At the present time, the geometry of the porous electrodes defies a complete description. We therefore assume the simplest reasonable model for the porous electrodes comprising a large number of uniform, long cylindrical tubes filled with the active material.

In this model, the electrical analogue of each 'pore' of the porous electrode is a distributed impedance of a uniform transmission-line type as characterized in Fig. 18.

If the ratio of pore length to pore diameter is large compared to unity, which is quite realistic in the case of sintered electrodes of the nickel–cadmium battery, the complex impedance of the active material-flooded porous tube is obtained from transmission-line theory as,

$$Z_0 = \sqrt{(Z_1 Z_2)}\,. \qquad (19)$$

It may be noted that R_Ω is outside the porous electrode structure and is therefore not a part of the distributed electrode impedance.

It is assumed that the electrode impedances of the anode and cathode are additive which is quite reasonable since they are not coupled in any other way. Since diffusion has been identified as a controlling factor, it may be assumed, following Warburg's theory of diffusional impedance that

$$Z_1 = (\sigma_1/\sqrt{\omega}) - j(\sigma_1/\sqrt{\omega}) \qquad (20)$$

where σ_1 is defined according to Equation 11 for the species diffusing along the axis of the pore. Such an expression for σ_1 is reasonable because the battery impedance is, in the present case, the value measured under near-equilibrium conditions. No terms due to polarization resistance or double-layer reactance are introduced in Z_1 because diffusion of the species along the long axis of the pore is not directly associated with charge-transfer or double-layer formation. On the other hand, modelling for Z_2 should take into account these factors too, since diffusion of the species occurs perpendicular to the pore wall at which charge-transfer also takes place. Since the Argand plots suggest predominant diffusion control, the charge-transfer resistance may be neglected compared to diffusional impedance so that we may write for the model of Z_2, as in Fig. 19

where

$$Z_2 = \{1/[(1/W_2) + j\omega\bar{C}]\} \qquad (21)$$

$$W_2 = (\sigma_2/\sqrt{\omega}) - j(\sigma_2/\sqrt{\omega}) \qquad (22)$$

and σ_2 is defined according to Equation 11 for the species diffusing (and reacting) normal to the pore wall, since the impedance values used here are again those under near equilibrium conditions.

As it has been demonstrated experimentally that diffusion is rate-controlling in the present case, it may be assumed that the Warburg impedance W_2 is much larger than the double-layer reactance $(-j/\omega\bar{C})$ in the experimental frequency range $\omega = 30$–200 rad s^{-1}.* Hence, the impedance Z_2 is approximately given as,

$$Z_2 \approx -(j/\omega\bar{C})\,. \qquad (23)$$

Substituting for Z_1 (Equation 20) and Z_2 (Equa-

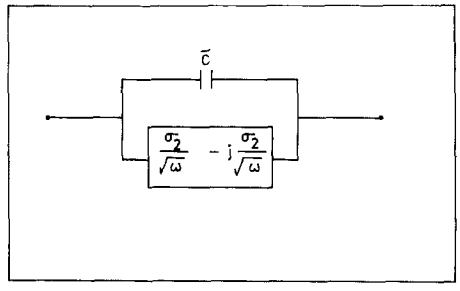

σ_2 = Warburg coefficient
ω = $2\pi f$, f = frequency (Hz)
$\bar{c}$ = Double layer capacitance
j = $\sqrt{-1}$

Fig. 19. Model of the equivalent circuit for the impedance Z_2 in Fig. 18 in the case of nickel–cadmium cell.

* This does not therefore correspond to the limit $\omega \to 0$ in Equation 8. The proper limit for the present case is $(\sigma/\sqrt{\omega}) \gg (1/\omega\bar{C})$.

tion 23) in Equation 19 for the electrode impedance Z_0, it follows that

$$Z_0 = \sqrt{\{[(\sigma_1/\sqrt{\omega}) - j(\sigma_1/\sqrt{\omega})]\ (-j/\omega\bar{C})\}}. \quad (24)$$

The right-hand side of Equation 24 may be evaluated using the identity,

$$\sqrt{(a \pm jb)} = \sqrt{\{[\sqrt{(a^2 + b^2)} + a]/2\}} \pm j\sqrt{\{[\sqrt{(a^2 + b^2)} - a]/2\}}. \quad (25)$$

It is thus found that

$$Z_0 = \left\{\frac{\sigma_1}{\omega^{3/2}\bar{C}}[(\sqrt{2} - 1)/2]\right\}^{1/2} - j\left\{\frac{\sigma_1}{\omega^{3/2}\bar{C}}[(\sqrt{2} + 1)/2]\right\}^{1/2} \quad (26)$$

The measured values of cell impedance $|Z|$, and its components R_s and C_s are therefore related to the fundamental parameters as,

$$|Z| = [R_s^2 + (1/\omega^2 C_s^2)]^{1/2} \quad (27)$$

$$NA\,R_s = R_\Omega + \sqrt{\{(\sigma_1/\omega^{3/2}\bar{C})\ [(\sqrt{2} - 1)/2]\}} \quad (28)$$

$$NA\,(1/\omega C_s) = \sqrt{\{(\sigma_1/\omega^{3/2}\bar{C})\ [(\sqrt{2} + 1)/2]\}} \quad (29)$$

where

N = number of cylindrical pores per unit area of the cell electrode, and
A = area of the electrode.

It follows from Equations 28 and 29 that:

(a) $(1/\omega C_s)$ versus $(1/\omega^{3/2})$ should be a straight line passing through the origin, and

(b) $(1/\omega C_s)$ versus R_s should be a straight line of slope 2·45 according to the equation $(1/\omega C_s) = \sqrt{6}\,(R_s - R_\Omega)$.

Figs. 14–16 show the plot of $(1/\omega C_s)$ versus $(1/\omega^{3/4})$ at different states-of-charge. Both the linearity and the location of the origin are supported by the data at all states of charge. However, as shown earlier (Fig. 13), $(1/\omega C_s)$ versus R_s is a straight line of slope 1·7 ± 0·1 which is substantially different from the value of 2·45 predicted by the new model. Nevertheless, in view of the good agreement with the theory as shown in Figs. 13–16, the model proposed above may be accepted as satisfactory. The possibility of a variable fractional power dependence of C_s on ω has been shown to exist also in a general treatment of impedance of flooded porous electrodes [16].

It may therefore be concluded that the model of the porous electrode of the sintered plate nickel–cadmium cell corresponding to the equivalent circuit of Fig. 20 is justified to a reasonable degree by the experimental data at all states of charge of the cell.

The experimental fact (Fig. 3) that the modulus of the impedance and equivalent series/parallel resistance of the battery have no detectable correlation with the state-of-charge may be now explained easily. Since R_Ω is a dominant term in R_s, it follows from Equations 27 and 28 that $|Z|$ as well as R_s (and therefore R_p too) will be masked by R_Ω, which gives no information on the state-of-charge.

A fairly useful correlation has been experimentally obtained only between C_s, C_p or ϕ and the state-of-charge (Figs. 6–8). An interpretation

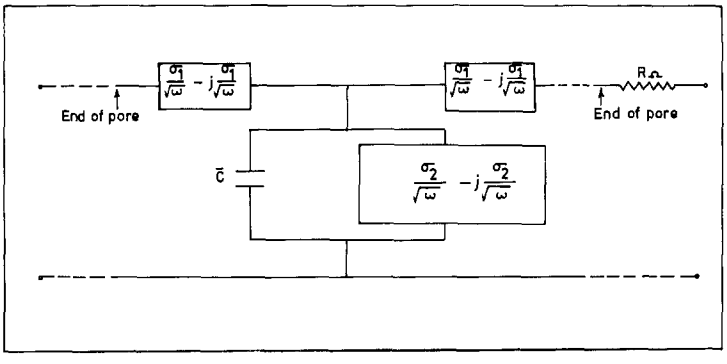

Fig. 20. Transmission-line model for the equivalent circuit of a single pore in the electrodes of a nickel–cadmium cell.

of this correlation may now be attempted on the basis of the model proposed above.

Consider Equation 29, the effective double-layer capacity $\bar{C}$ is proportional to the true area (A_2) of the metal–solution interface where charge transfer occurs and the Warburg coefficient σ_1 is inversely proportional to both the true cross-sectional area (A_1) through which the diffusion along the pore occurs, and also the concentration of the diffusing species (C_1^0). Thus, C_s is of the form

$$C_s \propto \sqrt{(A_1 A_2 C_1^0)} \qquad (30)$$

As far as the nickel–cadmium cell is concerned, the species that diffuse to and away from the porous electrode is the water molecule according to the cell (total) reaction

$$2\,H_2O_{(l)} + 2\,NiOOH_{(s)} + Cd_{(s)} \underset{\text{charge}}{\overset{\text{discharge}}{\rightleftharpoons}} 2\,Ni(OH)_{2(s)} + Cd(OH)_{2(s)} \,. \qquad (31)$$

The concentration C_1^0 is therefore relatively unchanged with a change in the state of charge. Hence,

$$C_s = k\sqrt{(A_1 A_2)} \qquad (32)$$

where k is a constant at a given alternating current frequency.

Consider an increase in the state-of-charge of the battery. The state of subdivision of the active materials, especially at the cadmium electrode, increases due to extensive nucleation. As a result, the terms A_1 and A_2 and therefore C_s will increase with the state-of-charge in some proportion. This trend is confirmed by experiment (Fig. 6).

The phase shift (ϕ) is given by $\tan^{-1}(1/\omega C_s R_s)$. Since the observed ϕ is quite small compared to unity, $\phi \approx (1/\omega C_s R_s)$. It has been shown that R_s is mainly composed of the solution resistance R_Ω. Hence, $\phi \approx (1/\omega C_s R_\Omega)$. In view of Equation 32,

$$\phi = [k'/(A_1 A_2)^{1/2}] \qquad (33)$$

where k' is a constant at a given alternating current frequency.

It is therefore to be expected in this case that the phase shift will decrease with an increase in the state of charge in some proportion. This trend is again confirmed (Fig. 8) by experiment.

Consider now the equivalent parallel capacitance C_p. Since the experimental data show that $\omega C_s R_s \gg 1$, at all states-of-charge, it follows from circuit theory that

$$C_p = [1/(\omega^2 C_s R_s^2)] \,. \qquad (34)$$

Substituting $R_s \approx R_\Omega$, $C_s = k\sqrt{(A_1 A_2)}$

$$C_p = [k''/(A_1 A_2)^{1/2}] \qquad (35)$$

where k'' is a constant at a given alternating current frequency. Hence C_p should decrease with an increase in the state-of-charge of the cell which is again confirmed by experiment (Fig. 7).

More useful correlations between the states-of-charge of the battery and the impedance parameters C_s, C_p and ϕ may be now derived by absorbing the frequency term in the measured variable from the corresponding equations. Thus, from Equations 29, 30, 32 and 33–35 it follows that

$$\omega^{1/4} C_s = k_0\sqrt{(A_1 A_2)} \qquad (36)$$

$$\omega^{3/4}\phi = k_0'/\sqrt{(A_1 A_2)} \qquad (37)$$

$$\omega^{5/4} C_p = k_0''/\sqrt{(A_1 A_2)} \qquad (38)$$

where the constants k_0, k_0' and k_0'' are independent of the alternating current frequency used for the measurement so long as the inductive effects are excluded, and $\sqrt{(A_1 A_2)}$ is proportional to some power of the state-of-charge of the cell or the battery.

Experimental results calculated according to Equations 36–38 at different frequencies and plotted against the state-of-charge of the cell are shown in Fig. 21.

It is thus established that at a given stage in the life of a nickel–cadmium cell, the state-of-charge may be predicted over a useful range by measuring C_p, C_s and ϕ at a sufficiently low alternating current frequency.

If the state-of-charge dependence of C_p, C_s or ϕ is mainly due to variations in the state of subdivision of the cadmium electrode as pointed out above, the quantitative aspects of the correlations will depend on the prior history of the cell to some extent. For example, a long-term storage or a large number of charge–discharge cycles which lead to a relatively coarse-grained structure of the cadmium electrode will influence the above correlations. Similarly, the degree of excess capacity used at the cadmium electrode for oxygen recombination during the overcharge will also effect the quantitative features of the correlations.

It is therefore concluded that a successful

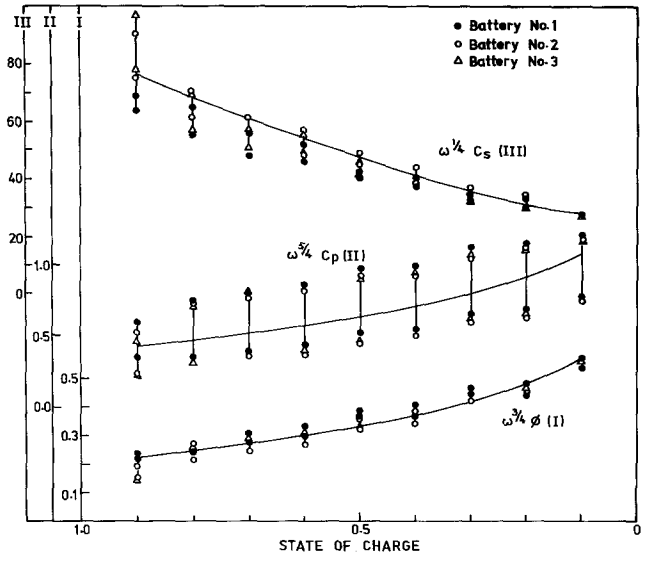

Fig. 21. Dependence of $\omega^{5/4} C_p$ (II), $\omega^{3/4}$ ϕ (I) and $\omega^{1/4} C_s$ (III) on state-of-charge independent of frequency (5–25 Hz).

non-destructive monitoring of the state-of-charge of a nickel–cadmium cell is practically feasible by the measurement of one of the quantities C_p, C_s or ϕ at a sufficiently low alternating current frequency, and then relating $\omega^{5/4} C_p$, $\omega^{1/4} C_s$ or $\omega^{3/4}\phi$ with the state-of-charge provided that a periodic calibration of the given type of cell is carried out after a deep charge–discharge conditioning cycle.

5. Conclusions

The impedance of a nickel–cadmium cell is predominantly controlled by diffusion.

The internal resistance is dominated by the resistance of the solution and separator between the electrodes and therefore not useful to characterize the state of charge of the cell.

Only the alternating current phase shift and equivalent series (or parallel) capacitance of the nickel–cadmium cell, when measured at sufficiently low a.c. frequencies, vary with the state-of-charge in a way useful for the prediction of the latter.

The impedance data obtained may be quantitatively interpreted using a model of the cell electrodes consisting of long cylindrical pores in which diffusion of ions occurs along the axis of the pore while both diffusion and charge transfer reactions occur at the interface between the pore wall and the active material.

The real factor underlying the observed correlation of the a.c. phase shift as well as of the equivalent series (or parallel) capacitance with the state-of-charge of the nickel–cadmium cell may be identified as due to the change in the double-layer capacitance at the pore wall and active material interface as a result of crystal nucleation and growth processes.

References

[1] S. Lerner, H. Lennon and H. Seiger, 'Power Sources', Vol. 3, (ed. D. H. Collins) Pergamon Press (1971) p. 135.
[2] H. Lurie, H. N. Seiger and R. C. Shair, *Proceedings of 17th Annual Power Source Conference* (1963) p. 110.
[3] R. H. W. Sieh, *Electrochim. Acta.* **13** (1964) 2139.
[4] J. J. Winter, J. Breslin, R. L. Ross and H. A. Leupold, *J. Electrochem. Soc.* **122** (1975) 1434.
[5] D. C. Jones, NTIS, US Department of Commerce Report No. AFAPL-TR-75-83 (1975).
[6] 'Eveready Battery Applications and Engineering Data', Copyright, Union Carbide Corp., New York (1971).
[7] W. J. Hammer, 'Primary Battery', Vol. 2, (eds. N. C. Cahoon and G. W. Heise), The Electrochemical Society USA (1976) p. 429.
[8] R. B. Naugle and A. W. Speyers, *Proceedings of 13th Annual Power Source Conference* (1959) p. 97.
[9] E. Dowgiallo and F. Belvoir, *Proceedings of the Annual Battery Workshop,* Goddard Space Flight Centre (1974) p. 32.
[10] A. Fleischer, 'Power Sources' Vol. 3 (ed. D. H. Collins) Pergamon Press (1971).

[11] N. Latner, *Rev. Sci. Inst.* **40** (1969) 364.
[12] R. R. Secunde and A. G. Birchenough, *Chem. Abstr.* **73** (1970) 83 023r.
[13] K. J. Euler, *Electrochim. Acta* **17** (1972) 619.
[14] S. Sathyanarayana, S. Venugopalan and M. L. Gopikanth, *J. Appl. Electrochem.* 8 (1978) 479.
[15] M. Sluyters-Rehbach and J. H. Sluyters, 'Electroanalytical Chemistry', Vol. 8 (ed. A. J. Bard) Marcel Dekker Inc, (1971) p. 157.
[16] S. K. Rangarajan, *J. Electroanalyt. Chem.* **22** (1969) 89.
[17] R. de Levie, 'Advances in Electrochemistry and Electrochemical Engineering' Vol. 6 (eds. P. Delahay and C. W. Tobias), Interscience (1967) p. 329.